Inter-user Frequency Offset Resilient Uplink FBMC by DFT Spreading and Cyclic Shift

Kwonhue Choi, *Senior Member, IEEE*

***Abstract*—We propose a new multiuser FBMC that performs cyclic-shift on DFT-spread data symbols prior to FBMC modulation. The interference between frequency asynchronous users' adjacent resource blocks (RBs) is minimized. In the receiver, the RBs' cyclic shift values are detected in a simple blind manner. As the inter-user frequency offset range increases, the conventional FBMC schemes break down, and the BERs saturate at high SNR. Moreover, with inter-user power differences, the BERs saturate to an unacceptable level. In contrast, the proposed FBMC retains the same slope of the BER curves as that of the interference-free case.**

***Index Terms*—FBMC, carrier frequency offset, multiple access**

I. Introduction

With the well frequency-localized pulse shaping filter of FBMC-OQAM (filter bank multicarrier with offset quadrature amplitude modulation), ideally, only one null (guard) subcarrier is required in between frequency-adjacent resource blocks (RBs) that are allocated to the different users of FBMC[1]-based uplink system [1, 2]. In practical uplink systems, there are typically different frequency offsets (FOs) among the users called *interuser FOs (IUFOs)* or *multiple FOs*. This is due to the inevitable mismatches among the users' transmit oscillators and the different Doppler shifts in mobile systems. In fifth-generation (5G) systems and beyond, much larger IUFOs need to be considered because of the higher Doppler shift by using mm-wave bands with higher mobility. In [3], the authors analyzed a frequency asynchronous FBMC system only with a non-fading channel, and the IUFO range was set very small. In [4], the authors only considered a *time*-asynchronous FBMC system while assuming zero IUFO.

If IUFOs are present, the band edge subcarriers of the frequency adjacent RBs allocated to the different users possibly overlap, and thus, inter-carrier interference (ICI) occurs. The discrete Fourier transform-spread (DFT-s) FBMCs have gained attention in recent literature for its low PAPR benefit [5, 6]. In this case, ICI is even more severe because the band edge subcarrier magnitudes can instantaneously be very large due to DFT spreading.

We can easily overcome ICI at the RB's band edge by simply inserting more null subcarriers [4]. However, this results in spectral inefficiency, which becomes critical when N denoting the number of subcarriers per RB is small for fine resource granularity, as in the case of Long Term Evolution (LTE) uplink, where N is 12. With $N = 12$, one more null subcarrier in between the frequency adjacent RBs results in about 7.7% bandwidth overhead. Therefore, it is crucial to devise a suitable scheme for uplink FBMC systems with large IUFOs. Thus, the main goal of this study is to propose a new frequency asynchronous FBMC scheme with substantially expanded tolerances of oscillator inaccuracy or Doppler shift. The contributions of this work are summarized as follows:

- A novel cyclic shift idea in conjunction with DFT-spreading is proposed for uplink FBMC systems.
- Unlike the previous works on uplink FBMC [3, 4, 7], the proposed scheme significantly increases the allowable IUFO range without wasteful guard subcarriers.
- The proposed scheme relaxes RF requirements such as oscillator accuracy and pre-compensation of Doppler shift, and does not require complicated algorithms for interuser interference cancellation.

Notations: DFT[$\mathbf{x}$] and IDFT[$\mathbf{x}$] denote the DFT and inverse DFT outputs of the vector $\mathbf{x}$, respectively, and $[f(n)]_{n=a}^{b}$ denotes $[f(a), f(a+1), \cdots, f(b)]^{\mathrm{T}}$.

II. Review on DFT-spread FBMC

Fig. 1 shows an uplink system model of the conventional multiuser DFT-s FBMC. The shaded blocks are added for the proposed scheme. We consider K frequency-adjacent RBs, which each contain N subcarriers (subchannels) and are allocated to one of K users. Without loss of generality, the kth RB is assumed to be allocated to the kth user. For high data rate service, the multiple RBs may be allocated to the same user and are placed apart with a distance larger than the bandwidth of K RBs for frequency diversity. Hence, the RB index k is used as a user index as well. The FBMC in-band subcarrier spacing is set to $1/T$ Hz, where T is the symbol duration. Let f_k denote the kth RB's (user's) up-conversion frequency as shown in Fig. 1. For one null subcarrier insertion between adjacent RBs, the adjacent RBs' up-conversion frequency difference, $f_{k+1} - f_k$, is set to $(N+1)/T$ Hz.

The only difference from the conventional (non-DFT-s) multiuser FBMC is that DFT spreading is performed prior to FBMC modulation and its counterpart, IDFT, is performed after FBMC demodulation. FBMC modulation and demodulation are well described in the literature [1], so the details on how they work are omitted here. In Fig. 1, $\mathbf{d}_{k,m}$ is the m-th $N \times 1$ data symbol vector of the kth RB, $\mathbf{x}_{k,m}$ is DFT$\left[\mathbf{d}_{k,m}\right]$, and $\mathbf{r}_{k,m}$ is FBMC demodulator output.

III. Proposed Scheme

A. Signal modification to DFT-spread FBMC

The elements of the DFT-spread data symbol vector have non-identical magnitudes, so the subcarriers of the DFT-s

The author is with the Department of Information and Communication Engineering, Yeungnam University, Gyeongsan 38541, Korea (e-mail: gonew@yu.ac.kr)

[1]Hereinafter, FBMC refers to FBMC-OQAM for simplicity.

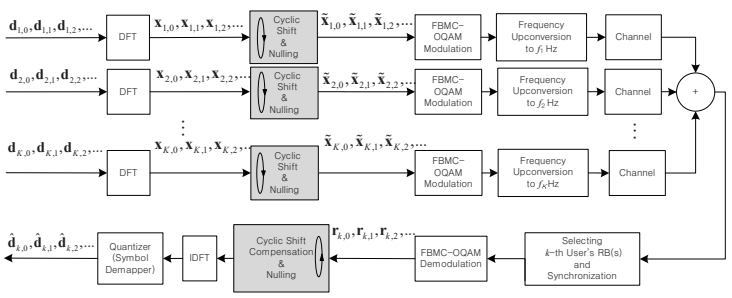

Fig. 1: System model of the proposed uplink multiuser FBMC scheme.

FBMC have non-identical magnitudes as well. One shot of the subcarrier magnitudes for adjacent RBs is illustrated at the top of Fig. 2. Despite one null subcarrier in between the RBs' bands, the subcarriers at each RB band edge interfere with the next RBs when there are different FOs among the RBs.

In the proposed scheme, the DFT-spread symbol vector $\mathbf{x}_{k,m}$ goes through a cyclic shift operation, as shown in Fig. 1 in order that a small magnitude element is shifted to the right-most element, as shown in Fig. 2. To do this, we first find the index of the local minimum magnitude element of $\mathbf{x}_{k,m}$ as follows:

$$s_{k,m} = \underset{n\in\{1,2,\cdots,N/4\}}{\operatorname{argmin}} \left|x_{k,m}(n)\right|, \quad (1)$$

where $x_{k,m}(n)$ denotes the nth element of $\mathbf{x}_{k,m}$. Then, to place this element at the right band edge, we cyclically shift $\mathbf{x}_{k,m}$ to the left by $s_{k,m}$ and obtain $\breve{\mathbf{x}}_{k,m}$ which is a cyclically shifted version of $\mathbf{x}_{k,m}$:

$$\breve{\mathbf{x}}_{k,m} = \underset{-s_{k,m}}{\text{CyclicShift}}\left\{\mathbf{x}_{k,m}\right\}, \quad (2)$$

where $\underset{k}{\text{CyclicShift}}\{\}$ denotes the k element cyclic shift operation. The search range in (1) is limited to the first quarter of the subcarrier indices (i.e., $\{1, 2, \cdots, N/4\}$) and not the whole range. This is to avoid ambiguity in the blind detection solution of $s_{k,m}$, which is explained in Section III-C.

When there are FOs among RBs, the ICI from a certain RB to the right-hand-side RB in the subcarrier axis is reduced by the proposed cyclic-shift idea. Meanwhile, as the left most subcarrier of each RB is not minimized, the ICI from the right-hand-side band RB to the considered RB is still significant. Hence, we exclude the right most subcarrier of each RB in the DFT despreading (IDFT) stage in the receiver because it is subject to severe interference. In the transmitter, we forcibly replace the right most subcarrier of each cyclic-shifted RB with zero, as shown at the bottom of Fig. 2 to generate FBMC modulation input denoted by $\tilde{\mathbf{x}}_{k,m}$ in Fig. 1. This is because we will not use the zero forced right most subcarrier in the DFT despreading in the receiver. By zero forcing right most subcarrier, we do not minimize but completely eliminate the ICI to the right-hand-side RB.

There is self-interference (SI) because the zero forced subcarrier is not included in the DFT despreading of the receiver. Let $\tilde{\mathbf{d}}_{k,m}$ denote the recovered version of $\mathbf{d}_{k,m}$ from $\tilde{\mathbf{x}}_{k,m}$ by

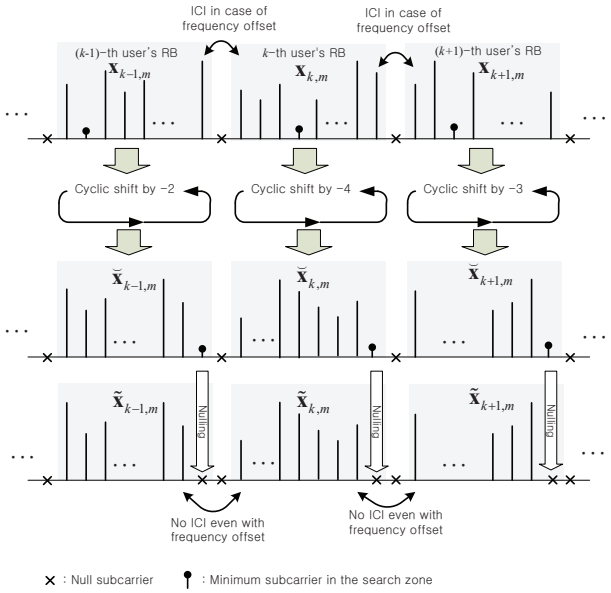

Fig. 2: Subcarrier domain signal modification for the proposed scheme.

compensating cyclic shift and performing DFT despreading, and let $\mathbf{e}_{k,m}$ denote the symbol magnitude-normalized SI term in $\tilde{\mathbf{d}}_{k,m}$. Then, $e_{k,m}(n) = (\tilde{d}_{k,m}(n) - d_{k,m}(n))/|d_{k,m}(n)|$. Table. I shows the variance and the maximum magnitude of $e_{k,m}(n)$, which are obtained by exhaustive calculation of $\mathbf{e}_{k,m}$ for all data symbol combinations of $\mathbf{d}_{k,m}$ for $N = 8$ and 16 and for 10^{10} random generations of $\mathbf{d}_{k,m}$ for $N = 32$. It is found that the variance of $e_{k,m}(n)$ is very small. This occurs because the zero forced subcarrier originally had the minimum magnitude in the search range and thus it has an insignificant contribution to DFT despreading. More remarkably, it is found that the maximum of $\left|e_{k,m}(n)\right|$ is smaller than 1. This implies that without background noise, the SI alone cannot make a symbol decision error for QPSK, and thus does not make an error floor in the high SNR region.

TABLE I: Variance and maximum magnitude of the normalized SI $e_{k,m}(n)$.

N	8	16	32
Variance of $e_{k,m}(n)$	0.066	0.0155	0.0037
Maximum of $\left\|e_{k,m}(n)\right\|$	0.8196	0.5957	0.3681

Intuitively, as N increases, the SI becomes negligible. Nonetheless, the large Ns are not the focus. This is because the RB size N is commonly set small for fine resource granularity like LTE uplink. Moreover, for large Ns, simply inserting more than one null in between adjacent RB bands is a trivial and reasonable solution for combatting the IUFO. For instance, even with N=32, one more null insertion results in only a 3% bandwidth overhead.

B. Blind detection of $s_{k,m}$

In Fig. 1, $\mathbf{r}_{k,m}$ denotes the FBMC demodulated counterpart to $\tilde{\mathbf{x}}_{k,m}$ of the transmitter. We discard the right most subcarrier because it has been forced to zero in the transmitter, and thus, we set $r_{k,m}(N) = 0$. For subsequent correct demodulation, the cyclic shift should be compensated prior to the DFT

despreading (IDFT) stage, as shown in Fig. 1. Thus, the receiver should know the shift variable, $s_{k,m}$. In the proposed scheme, $s_{k,m}$ is detected in a blind way based on the tentative decision variables.

Let $\mathbf{t}_{k,m}^{(l)}$ denote the tentative decision variable vector (quantizer input in Fig. 1) for $\mathbf{d}_{k,m}$ where l is a trial value of $s_{k,m}$. Then $\mathbf{t}_{k,m}^{(l)}$ is calculated as follows:

$$\mathbf{t}_{k,m}^{(l)} = \text{IDFT}\left[\underset{l}{\text{CyclicShift}}\left\{\mathbf{r}_{k,m}\right\}\right]. \tag{3}$$

Cyclic-shifting in the frequency domain is equivalent to multiplying the signal by a complex sinusoid in the time domain. Using this property, we change (3) as follows:

$$\begin{aligned}\mathbf{t}_{k,m}^{(l)} &= \text{IDFT}\left[\mathbf{r}_{k,m}\right] \odot \left[e^{\text{j}\frac{ln2\pi}{N}}\right]_{n=0}^{N-1} &(4)\\ &= \text{IDFT}\left[\underset{s_{k,m}}{\text{CyclicShift}}\left\{\mathbf{r}_{k,m}\right\}\right] \odot \left[e^{\text{j}\frac{(l-s_{k,m})n2\pi}{N}}\right]_{n=0}^{N-1} &(5)\end{aligned}$$

where $\odot$ denotes element-wise multiplication. The term $\text{IDFT}\left[\underset{s_{k,m}}{\text{CyclicShift}}\left\{\mathbf{r}_{k,m}\right\}\right]$ corresponds to the decision variable vector by the correct cyclic shift compensation by $s_{k,m}$. Thus, its elements are distributed around the data symbol constellation points (i.e., $\pm1\pm$j assuming QPSK). From (5), we know that with $l \neq s_{k,m}$, the tentative decision variable vector $\mathbf{t}_{k,m}^{(l)}$ has a residual carrier offset $\left[\exp\left\{\text{j}(l-s_{k,m})n2\pi/N\right\}\right]_{n=0}^{N-1}$. Then, its complex-valued element $t_{k,m}^{(l)}(n)$ rotates as the symbol index n increases, and thus, it stays off the constellation points. Based on this result, the blind estimate of $s_{k,m}$ denoted by $\hat{s}_{k,m}$ is obtained by calculating and comparing the norm of the quantized error vectors for the different l's as follows:

$$\hat{s}_{k,m} = \underset{l\in\{1,2,\cdots,N/4\}}{\text{argmin}} \left\|\mathbf{t}_{k,m}^{(l)} - \mathbf{t}_{k,m}^{(l)\boxplus}\right\|^2 \tag{6}$$

where $\mathbf{t}_{k,m}^{(l)\boxplus}$ denotes the quantized (QPSK or QAM-demapped) version of $\mathbf{t}_{k,m}^{(l)}$. Recall that $s_{k,m}$ in (1) is the local minimum index in the limited region $l \in \{1,2,\cdots,N/4\}$. Hence, the candidates of $\hat{s}_{k,m}$ in (6) are also limited to this region.

If we use (3) in the calculation of (6), $N/4$ IDFT operations and $N/4$ N-sized vector norm operations are needed. To circumvent this high-computation-complexity problem, we employ (4) instead of (3). Then, we need the IDFT operation only once and additionally $N/4-1$ element-wise multiplications of N-sized vectors. Adding the vector norm operations to this, the total number of complexity multiplications (CMs) for the blind detection of $s_{k,m}$ is just $(N/2)\log_2 N + N^2/2 - N$. For small Ns, the complexity is substantially smaller than the basic demodulation complexity of DFT-s FBMC given as $(2\kappa + 9/2\log_2 N + 10)N$ CMs [5], where κ denotes the pulse-shaping filter overlapping factor. For instance, with κ=4, the complexity overheads of the proposed schemes with $N = 8$ and 16 are 14% and 25%, respectively.

In the selective fading channel, the channel magnitude inverted FBMC demodulator output $\mathbf{r}_{k,m}$ invokes noise enhancement in the DFT despread output $\mathbf{t}_{k,m}^{(l)}$. Thus, the norm of the quantized error vectors in (6) undergoes noise enhancement as well. As a more reliable method, we can use an intermediate signal which is free from noise enhancement. To do this, we express the FBMC demodulated symbol vector $\mathbf{r}_{k,m}$ as follows:

$$\mathbf{r}_{k,m} = \mathbf{i}_{k,m} \odot \mathbf{f}_{k,m} \tag{7}$$

where $\mathbf{f}_{k,m}$ is an intermediate FBMC demodulated symbol vector with non-inverted channel magnitude, and $\mathbf{i}_{k,m}$ is a per-carrier channel magnitude inversion vector. To avoid noise enhancement, we use $\mathbf{f}_{k,m}$ instead of $\mathbf{t}_{k,m}^{(l)}$ in (6). Then, we use the following rule instead of (6):

$$\hat{s}_{k,m} = \underset{l\in\{1,2,\cdots,N/4\}}{\text{argmin}} \left\|\mathbf{f}_{k,m} - \tilde{\mathbf{f}}_{k,m}^{(l)}\right\|^2 \tag{8}$$

where $\tilde{\mathbf{f}}_{k,m}^{(l)}$ is a reconstructed estimate of $\mathbf{f}_{k,m}$ from the tentative quantized output $\mathbf{t}_{k,m}^{(l)\boxplus}$ as follows: $\tilde{\mathbf{f}}_{k,m}^{(l)} = \mathbf{h}_{k,m} \odot \underset{-l}{\text{CyclicShift}}\left\{\text{DFT}\left[\mathbf{t}_{k,m}^{(l)\boxplus}\right]\right\}$.

The simulation results reveal that the scheme using (8) performs better than the scheme using (6), especially for a small N. This is because a smaller N results in a less reliable decision variable $\mathbf{t}_{k,m}^{(l)}$ in (6) due to the lower frequency diversity and larger SI as a result of the zero forced subcarrier. Thus, the reliability enhancement by the scheme using (8) is more effective in a system with small N compared to one with large N. The scheme using (8) additionally requires $N/4$ element-wise multiplications and DFTs, but the complexity overhead is acceptable for small N. If $N = 8$, then $N/4 = 2$, which means that signal reconstruction is needed only two times. Moreover, the basic computation complexity is small for small N.

C. Ambiguity of the solution for $s_{k,m}$

Suppose that we extend the search range of l in (6) (i.e., $[1,2,\cdots,N/4]$) to the entire range of subcarrier indices. We can express a set of l, $\{1,2,\cdots,N\}$ as $\{l = (N/4)p + q | p \in \{0,1,2,3\}, q \in \{1,2,\cdots N/4\}\}$. Then, the complexity sinusoid, $e^{\text{j}\frac{ln2\pi}{N}}$ in (4), is rewritten as $e^{\text{j}\frac{(N/4)pn2\pi}{N}} e^{\text{j}\frac{qn2\pi}{N}}$, where $e^{\text{j}\frac{(N/4)pn2\pi}{N}}$ is simplified as $e^{\text{j}pn\pi/2} = \text{j}^{pn}$. Hence, substituting $\text{j}^{pn} e^{\text{j}\frac{qn2\pi}{N}}$ into $e^{\text{j}\frac{ln2\pi}{N}}$ in (4), $\mathbf{t}_{k,m}^{(l)}$ in (4) is equal to $\text{j}^{pn}\mathbf{t}_{k,m}^{(q)}$, and then its quantized version is equal to $\text{j}^{pn}\mathbf{t}_{k,m}^{(q)\boxplus}$. Substituting these results into (6), $\left\|\mathbf{t}_{k,m}^{(l)} - \mathbf{t}_{k,m}^{(l)\boxplus}\right\|$ is given as $\left\|\text{j}^{pn}\mathbf{t}_{k,m}^{(q)} - \text{j}^{pn}\mathbf{t}_{k,m}^{(q)\boxplus}\right\| = |\text{j}^{pn}| \left\|\mathbf{t}_{k,m}^{(q)} - \mathbf{t}_{k,m}^{(q)\boxplus}\right\|$ which is equal to $\left\|\mathbf{t}_{k,m}^{(q)} - \mathbf{t}_{k,m}^{(q)\boxplus}\right\|$ because $\text{j}^{pn} = \pm1$ or $\pm j$ and $|\text{j}^{pn}|=1$. This implies that for the four different l's whose q values in the form of $p(N/4)+q$ are identical, the error term $\left\|\mathbf{t}_{k,m}^{(q)} - \mathbf{t}_{k,m}^{(q)\boxplus}\right\|$ is also identical and this results in four multiple solutions for $s_{k,m}$ in (6). This explains why, we limit the range of $s_{k,m}$ to $[1, N/4]$ in (1).

IV. Simulation Results

The system parameters and the channel environments were set as follows. For FBMC pulse shaping, a PYHYDYAS pulse with κ=4 was employed [1]. The subcarrier spacing was set to 15 kHz as in LTE uplink, and each RB from

the different users had an independent FO. In other words, there were different FOs among the users. Specifically, the kth RB's center frequency f_k in Fig. 1 was set to 15e3 $\times\{(N+1)(k-1)+\epsilon_k\}$ Hz, where ϵ_k is a normalized FO that is independent and identically distributed (i.i.d.) for different values of k and is uniformly distributed over $[-\Delta_f \ \ \Delta_f]$. Two typical multipath fading channels, ITU-R Pedestrian A and ITU-R Vehicular A were considered. For per-carrier channel magnitude inversion vector $\mathbf{i}_{k,m}$ in (7), the minimum mean-squared error (MMSE) criterion was employed. To include the nonidentical received powers among the RBs due to shadow fading or imperfect power control among the uplink users, the long-term scale factor $10^{S_k/10}$ was multiplied with the k-th RB's received power, where S_k is a zero mean real Gaussian random variable with standard deviation σ_s and is i.i.d. for different values of k.

Fig. 3 shows the simulated BERs of the conventional DFT-s FBMC and the proposed scheme when the data symbol vector $\mathbf{d}_{k,m}$ in Fig. 1 is QPSK-modulated with $N = 8$ and 16, $K = 8$, $\Delta_f = 0.8$, and $\sigma_s = 0$ and 6. For the blind detection of cyclic shift $s_{k,m}$, (6) and (8) are employed for $N = 16$ and 8, respectively. For reference, the BERs of the pure (non-DFT-s) FBMC are also included. In all cases, as σ_s increases to 6, the BER performance severely degrades, and the BERs at E_b/N_0 as high as 15 dB increase to larger than 10^{-2}. These large uncoded BERs are unacceptable even with commonly used channel coding schemes, especially for stable data service, which requires an uncoded BER of less than 10^{-3}. Therefore, the BER performance comparison at these large BER levels is not so meaningful.

Even in a high SNR region, the conventional DFT-s FBMC and the pure FBMC severely deteriorate, irrespective of σ_s and the BERs saturate. This occurs because the interuser ICI from IUFO is dominant over the background noise. In contrast, the proposed scheme fairly maintains the slope of the BER curves and thus achieves much lower BER than the conventional schemes. This confirms that the proposed cyclic shift technique suppresses the interuser ICI well.

Fig. 4 shows BER as a function of Δ_f for several values of σ_s. For neat presentation, the results for pure FBMC are excluded, and the trends can be conjectured from Fig. 3. Note that as σ_s increases, the performance-crossing point of Δ_f beyond which the proposed scheme outperforms the conventional DFT-s FBMC becomes smaller. This implies that even small IUFO is detrimental to the conventional DFT-s FBMC for larger power differences among the users.

Summing up, the proposed scheme performs better than the conventional FBMC and DFT-s FBMC as Δ_f and δ_s increase. As Δ_f and δ_s vary relatively slowly, it is feasible to switch between the conventional schemes and the proposed scheme according to these parameters, which will further improve the performance. Switching between the schemes is accomplished by simply including or excluding the cyclic shift operation (and its compensation operation) in Fig. 1.

V. Conclusions

We have proposed a new frequency asynchronous multiuser FBMC scheme that allows for substantially expanded tolerances of oscillator inaccuracy or Doppler shift. The proposed scheme is expected to reduce the cost of RF and baseband integrated circuits (ICs) by relaxing RF requirements. We expect the proposed scheme to be a promising solution considering that asynchronism is one of the key issues in 5G systems and beyond.

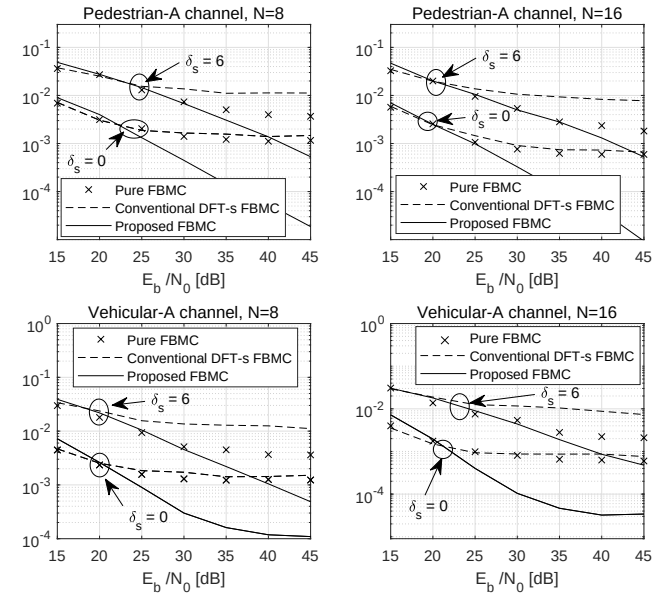

Fig. 3: BER curves of the pure FBMC, conventional DFT-s FBMC and proposed scheme, QPSK, Δ_f=0.8.

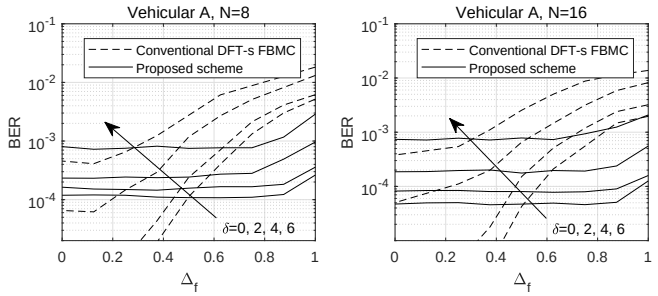

Fig. 4: BERs for conventional DFT-s FBMC and the proposed scheme, E_b/N_0=40 dB.

References

[1] M. Bellanger *et al.*, "FBMC physical layer: A primer," *PHYDYAS*, Jun. 2010. [Online] Available: http://www.ictphydyas.org/teamspace/

[2] D. Gregoratti and X. Mestre, "Uplink FBMC/OQAM-based multiple access channel: Distortion analysis under strong frequency selectivity," *IEEE Trans. Signal Process.*, vol. 64, no. 16, pp. 4260-4272, Aug. 2016.

[3] T. Fusco, A. Petrella, and M. Tanda, "Sensitivity of multi-user filterbank multicarrier systems to synchronization errors," in *Proc. IEEE Int. Symp. Commun. Control Sig. Process*, Mar. 2008, pp. 393-398.

[4] V. Berg, J. B. Dore, and D. Noguet, "A multiuser FBMC receiver implementation for asynchronous frequency division multiple access," in *Proc. Euromicro Conf. on Digital Syst. Design*, Aug. 2014, pp. 16-21.

[5] D. Na and K. Choi, "Low PAPR FBMC," *IEEE Trans. Wireless Commun.*, vol. 17, no. 1, pp. 182-193, Jan. 2018.

[6] K. Choi, "Alamout coding for DFT spreading-based Low PAPR FBMC," *IEEE Trans. Wireless Commun.*, vol. 18, no. 2, pp. 926-941, Feb. 2019.

[7] Y. Cheng, P. Li, and M. Haardt, "FBMC/OQAM for the asynchronous multi-user MIMO uplink," in *Int. ITG Workshop Smart Antennas*, Mar. 2014. pp. 1-6.